Microstructure and anodic polarization behavior of experimental Ag–18Cu–15Pd–12Au alloy in aqueous sulfide solution

KAZUHIKO ENDO, HIROKI OHNO
Department of Dental Materials Science, School of Dentistry, Health Sciences University of Hokkaido, 1757 Kanazawa, Tobetsu-cho, Ishikari-gun, Hokkaido 061-0293, Japan

SHUKUJI ASAKURA
Division of Materials Science and Chemical Engineering, Faculty of Engineering, Yokohama National University, 156 Tokiwadai, Hodogaya-ku, Yokohama-shi, Kanagawa 240-8501, Japan

The anodic corrosion behavior of an experimental Ag–15Pd–18Cu–12Au alloy in 0.1% Na_2S solution in relation to its microstructure was investigated using potentiodynamic and potentiostatic polarization techniques with analyses of corrosion products by X-ray diffractometry, Auger electron spectroscopy, and X-ray photoelectron spectroscopy. The role of Pd in improvement of the corrosion resistance was also investigated.

In the potential/current density curve, three distinct current peaks, at -520 mV (peak I), -425 mV (peak II) and -175 mV (peak III), were observed. The Ag-rich α_2 matrix with coarse Cu and Pd-rich lamellae was the most corrosion-susceptible region, and this region was preferentially corroded at peak I with the formation of granular deposits of Ag_2S. A small amount of Ag–Cu mixed sulfide deposited on the Cu and Pd-rich coarse particles and dissolution of Ag as AgO^- might have occurred in parallel with Ag_2S formation at peak II. Enrichment of Pd on the alloy surface occurred at peak III due to preferential dissolution of Ag and Cu. A high level of corrosion resistance was attained with the formation of a thin Pd-rich sulfide film, which enhanced the passivity of the alloy in an alkaline sulfide solution. It was found that passivity is an important phenomenon not only for base metal alloys but also for noble metal alloys to maintain high levels of resistance to corrosion and tarnishing in sulfide environments.

1. Introduction

Ag–20Pd–(10–20)Cu–12Au alloys have been widely used in Japan as alternatives to expensive Au casting alloys for cast inlays, crowns and bridges because the cost of dental treatment using an Ag-based alloy, but not that using an Au-based alloy, is covered by the national health insurance. The properties of Ag-based alloys generally satisfy the requirements of a dental casting alloy, but these alloys are more susceptible than are Au-based alloys to corrosion and tarnishing, especially in the presence of sulfide and hydrogen sulfide ions [1, 2].

The corrosion behavior the Ag-based alloys in sulfide solutions has mainly been investigated from the view point of assessment of susceptibility to tarnishing by means of microscopical observations of the attacked component phases or measurement of the color vector change due to the formation of insoluble corrosion products [3–7]. Niemi and Holland [3] examined the attacked structural components of an Ag–24.5Pd–13.5Cu–5.3Au alloy after exposure to an aqueous 2% Na_2S solution using SEM and light optical microscopy, and they found that Cu- and Pd-rich components had greater resistance to corrosion than did the Ag-rich component. German *et al*. [5] evaluated the resistance to tarnishing of 11 commercial noble metal alloys, including Ag-based alloys, with different noble metal contents and demonstrated that below approximately 55 at % noble metal (Au, Pt, and Pd) content, microstructure plays a dominant role in determination of resistance to tarnishing.

Although the electrochemical potentiodynamic polarization technique can provide useful information on corrosion behavior over a wide range of potentials, there have been few studies in which this technique was used to investigate the corrosion of Ag-based alloys in sulfide solutions. In a previous study, we obtained the potentiodynamic polarization curves for commercial Ag–Pd–Cu–Au alloys with different compositions in 0.1% Na_2S solution and demonstrated that the anodic current density peaks observed between -500 and -375 mV (vs. Ag/AgCl) became smaller with an increase in Au content [8]. Iijima *et al*. [9] also reported

that the anodic current density for an Ag–20.1Pd–16.5Cu–12.1Au alloy in 0.1% Na_2S solution in the potential range of 0 to +500 mV (vs. Ag/AgCl) was markedly larger than that for an Ag–20.8Pd–17.9Cu–18.3Au alloy, and they concluded that the addition of Au improved the resistance to corrosion and tarnishing in a sulfide environment. Holland demonstrated that the potentiodynamic polarization curve for an Au–31Ag–9.4Cu–4.1Pd–1.0In alloy in 2% Na_2S solution was markedly different from that in artificial saliva [10]. Several characteristic current density peaks were observed in those anodic polarization curves, but the assignment of reactions that occurred at potentials at which these current density peaks were observed has not been completely accomplished.

The present study was designed to obtain a more thorough understanding of the anodic polarization behavior of dental Ag–Cu–Pd–Au alloys in 0.1% Na_2S solution in relation to their microstructure. We employed an experimental Ag–18Cu–15Pd–12Au alloy, and the reactions involved at different potentials were investigated on the basis of the thermodynamic data and by analyses of corrosion products using X-ray diffractometry (XRD), Auger electron spectroscopy (AES), and X-ray photoelectron spectroscopy (XPS) after potentiostatic polarizations. The role of Pd in improvement of the corrosion resistance was also investigated.

2. Experimental method

2.1. Materials

A Ag–18Cu–15Cu–12Au (mass %) alloy ingot was made from metals with purities of more than 99.9% in a high-frequency induction furnace under an Ar gas atmosphere. The alloy was cast in a $12 \times 12 \times 1 mm^3$ plate by a vacuum/pressure casting machine. After casting, the alloy specimens in a gypsum-based mold were bench-cooled to room temperature. The surface of the specimen was metallographically polished with SiC papers and then by 3 μm Al_2O_3 paste. The polished specimens were cleaned ultrasonically in deionized water for 1 min and then dried with oil-free compressed air.

2.2. Metallurgical examination

The polished alloy was etched in an aqueous solution containing 5% KCN and 5% $(NH_4)_2S_2O_8$, washed with deionized water, and then dried with compressed air. The microstructure of the alloy was examined using an electron probe microanalyzer. The crystal structure of the alloy was examined using an X-ray diffractometer with Ni-filtered Cu K_α-radiation generated by 35 kV accelerating voltage and 20 mA anode current. The diffraction pattern was obtained with a scanning speed of $1^\circ(2\theta) \cdot min^{-1}$.

2.3. Electrochemical corrosion tests

2.3.1. Potentiodynamic polarization measurement

Anodic potentiodynamic polarizations of the Ag–18Cu–15Pd–12Au alloy were carried out in deaerated 0.1% Na_2S solution ($[Na_2S] = 1.3 \times 10^{-2}$M, pH = 12). A Ag/AgCl electrode (saturated KCl) was used as the reference electrode and a Pt wire was used as the counter electrode. A fresh solution was made for each measurement and was deaerated by bubbling ultrapure Ar gas for at least 60 min before sample introduction in the cell and throughout the period of the potentiodynamic polarization measurement. The potentiodynamic polarization was started from the free corrosion potential at a scan rate of $0.17 mV \cdot S^{-1}$. Anodic potentiodynamic polarizations of pure Au and a commercial alloy (Ag 49%, Pd 20%, Cu 18%, Au 12%, others 1%) were also carried out for comparison. The electrochemical cell temperature was always kept at $37 \pm 0.5\,^\circ C$.

2.3.2. Potentiostatic polarization testing

The electrode potential of the alloy specimen was maintained in deaerated 0.1% Na_2S solution at specific potentials at which distinct current peaks were observed in a potential/current density curve. The surface of the alloy specimen after the potentiostatic polarization was observed by a scanning electron microscope to examine the corrosion morphology. The corrosion products that had formed on the alloy specimen were analyzed by XRD. An X-ray diffractometer (2013, Rigaku Co. Ltd., Tokyo, Japan) with Ni-filtered Cu K_α-radiation (35 kV, 20 mA) was used. The patterns were recorded with a scanning speed of $1^\circ(2\theta) \cdot min^{-1}$. Small corrosion products of approximately 0.5 μm in diameter were analyzed using an Auger electron spectrometer (Model 650, Perkin Elmer, Norwalk, USA). Auger spectra were obtained at 20 kV electron beam voltage and 4.4 nA electron current with a beam diameter of 20 nm. The low electron beam current was intended to minimize sample damage. The surface of the alloy after potentiostatic polarization was also examined by XPS. XPS spectra were obtained using an XPS (ESCA-850, Shimadzu Co. Ltd., Kyoto, Japan) with Al K_α-radiation operated at 7 kV accelerating voltage and 30 mA current under a vacuum of 1×10^{-6}Pa. The binding energy scale was calibrated by the Au $4f_{7/2}$ and Cu $2p_{3/2}$ peaks at 83.8 and 932.8 eV, respectively.

3. Results

3.1. Microstructure

Fig. 1 shows a secondary electron image of the etched Ag–18Cu–15Pd–12Au alloy in an as-cast condition and characteristic X-ray images of Ag L_α, Cu K_α, and Pd L_α. The alloy consisted of four different microconstituents: coarse particles with irregular shapes (a), Widmanstätten precipitates (b), fine and coarse precipitate lamellae (c), and matrix. Microprobe analyses showed that the coarse particles were rich in Cu and Pd and depleted in Ag. A characteristic X-ray image of Au K_α showed that there had been no segregation and that the Au was evenly distributed throughout the alloy structure. Fig. 2 shows the X-ray diffraction pattern of the Ag–18Cu–15Pd–12Au alloy in an as-cast condition. The diffraction peaks for the three phases, Cu-rich fcc α_1, Ag-rich fcc α_2 and bcc PdCu β ordered phases, can be seen in the figure.

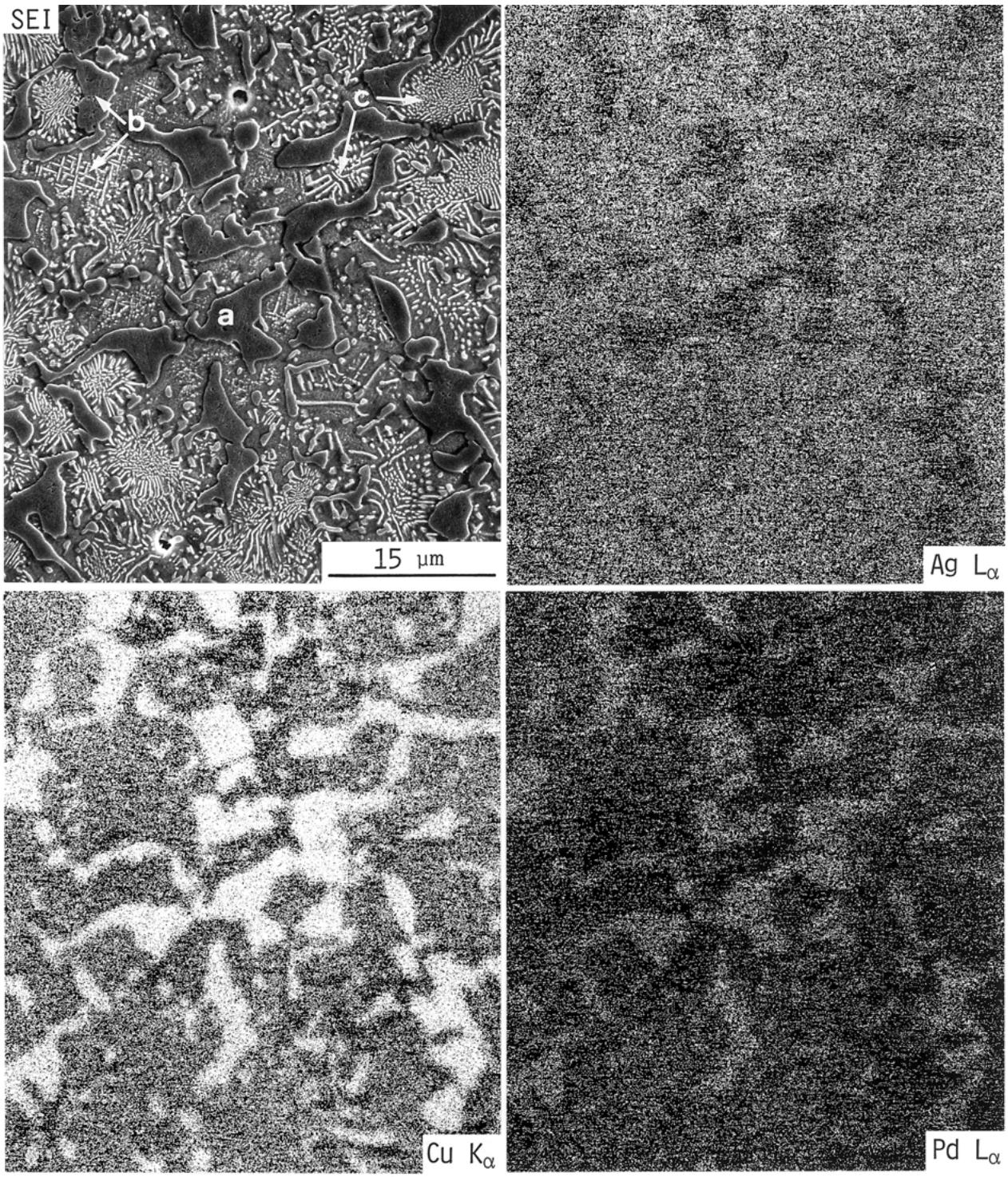

Figure 1 Secondary electron image of the etched Ag–18Cu–15Pd–12Au alloy and characteristic X-ray images of Ag K_α, Cu K_α and Pd L_α.

3.2. Potentiodynamic polarization behaviors in 0.1% Na_2S solution

Fig. 3 shows the anodic potential/current density curves for the Ag–18Cu–15Pd–12Au alloy together with the curves for the commercial Ag–20Pd–18Cu–12Au alloy and pure Au. Three distinct current density peaks were observed for the Ag–18Cu–15Pd–12Au and the commercial alloys: at −520 mV (peak I), at −425 mV (peak II), and at −175 mV (peak III). The values of the three current density peaks for the Ag–18Cu–15Pd–12Au alloy were all larger than those for the commercial alloy. The broad peak III was also observed for pure Au.

3.3. Surface analyses after potentiostatic polarizations

Fig. 4 shows secondary electron images of the alloy surface after potentiostatic polarization at each of peaks I (a), II (b) and III (c) for 15 min. At peak I, crystalline corrosion products formed on the specific area of the Ag-rich matrix, while few corrosion products formed on the Cu and Pd-rich coarse particles. At peak II, the amount of corrosion products on the Ag-rich matrix was markedly smaller than that at peak I, and small deposits were also observed on the Cu and Pd-rich coarse particles. At peak III, the amount of corrosion products

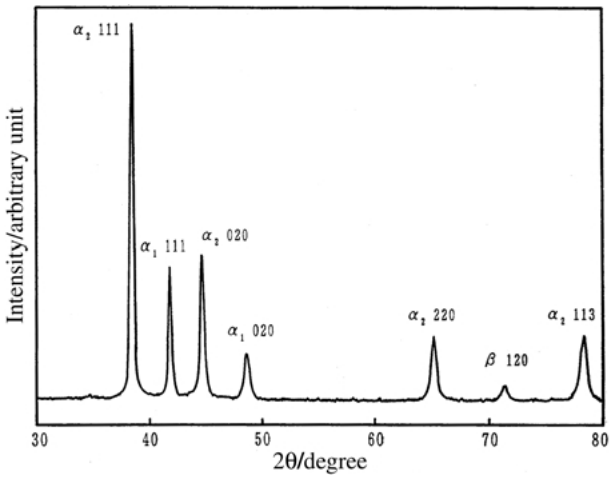

Figure 2 X-ray diffraction pattern for the polished Ag–18Cu–15Pd–12Au alloy in an as-cast condition.

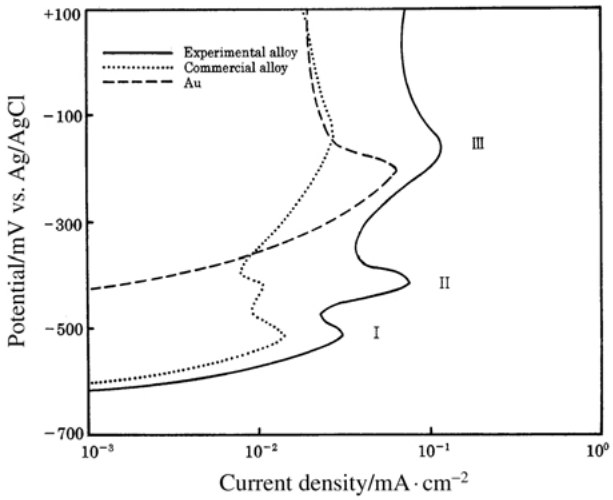

Figure 3 Potential/current density curves of the Ag–18Cu–15Pd–12Au alloy, commercial alloy, and the Au electrode in a deaerated 0.1% Na_2S solution.

was much smaller than the amounts at the other two peaks.

Fig. 5 shows the X-ray diffraction pattern obtained from the alloy surface after polarization at peak I, displaying the diffraction peaks for Ag_2S. Although small corrosion products were formed on Cu and Pd-rich components at peak II, neither Cu sulfide nor Pd sulfide were detected by X-ray diffraction on the alloy surface polarized at peak II. Then the small corrosion products formed on Cu and Pd-rich particles (microconstituent (a) in Fig. 1) during the polarization at peak II were analyzed by point analysis using AES. Fig. 6 shows an AES survey spectrum of a single small corrosion product of approximately 0.5 μm in diameter. A large S peak is observed with peaks for alloying elements, Ag and Cu. The fact that peaks for Au and Pd were not evident indicates that AES signals from the alloy substrate under the small corrosion product were not involved in the survey spectrum. A quantitative analysis of the elements indicated that the corrosion product was most likely to be $Ag_{1.2}Cu_{0.8}S$.

Fig. 7 shows the relative concentrations of S and the alloying elements (at %) on the alloy surface after potentiostatic polarization for 15 min at each peak (peaks I–III) obtained from quantitative analysis by XPS. The surface concentration of S was the highest at all three potentials. A drastic increase in Pd concentration was observed at peak III, accompanying decreases in Ag and Cu concentrations compared to their concentrations at peaks I and II. The concentration of Au increased slightly as the electrode potential increased. In order to examine the chemical state of the enriched Pd and S at peak III, high-resolution Pd 3d and S 2p spectra were obtained, and the results are shown in Fig. 8(a) and (b). The Pd 3d spectrum revealed two chemical states of Pd, metallic Pd (Pd^0) and Pd^{2+}. The S 2p spectrum also revealed two chemical states, one corresponding to metal sulfide (S^{2-}) and one corresponding to adsorbed elemental sulfur (S^0).

4. Discussion

4.1. Microstructure of the experimental Ag–18Cu–15Pd–12Au alloy

Microstructually, the constituent phases of the experimental Ag–18Cu–15Pd–12Au alloy were the Cu-rich fcc α_1, Ag-rich fcc α_2, and bcc PdCu β ordered phases. These constituent phases were the same as those for the commercial Ag–20Pd–(10–20)Cu–12Au casting alloys

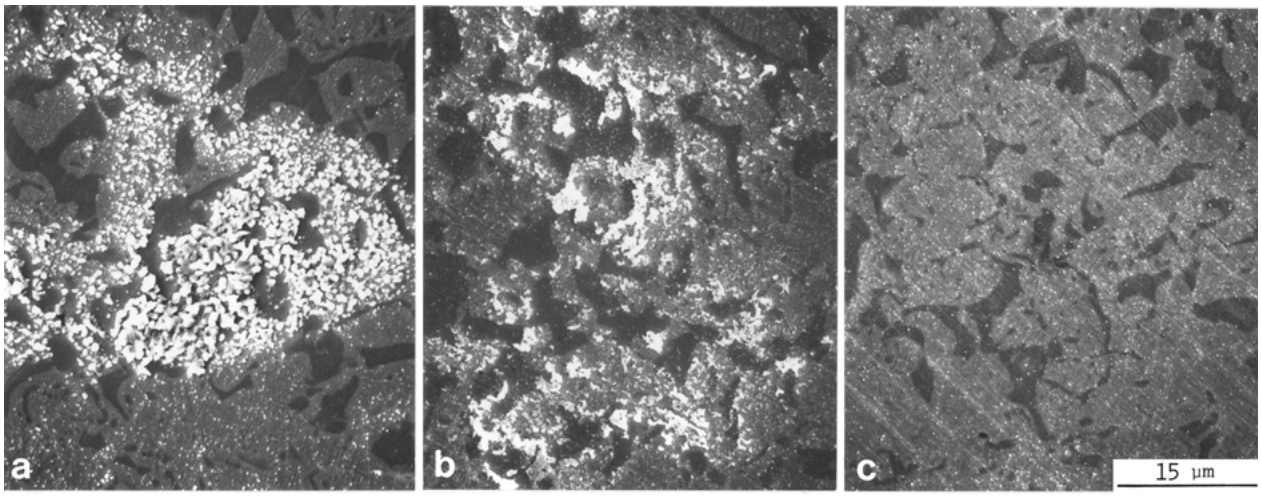

Figure 4 Secondary electron images of the Ag–18Cu–15Pd–12Au alloy surface after potentiostatic polarization for 15 min at − 520 mV (a), − 425 mV (b) and − 175 mV (c).

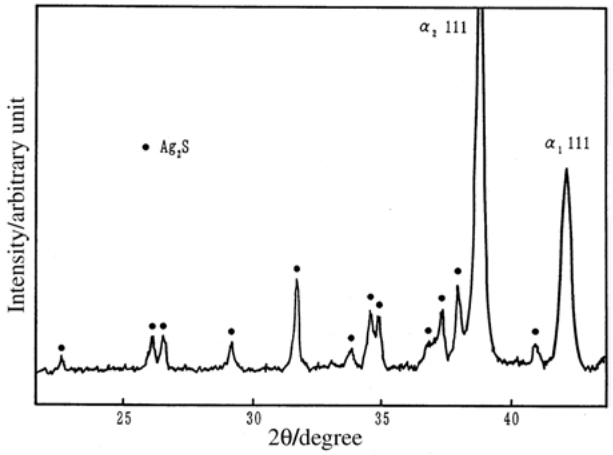

Figure 5 X-ray diffraction pattern for the Ag–18Cu–15Pd–12Au alloy after potentiostatic polarization at − 520 mV.

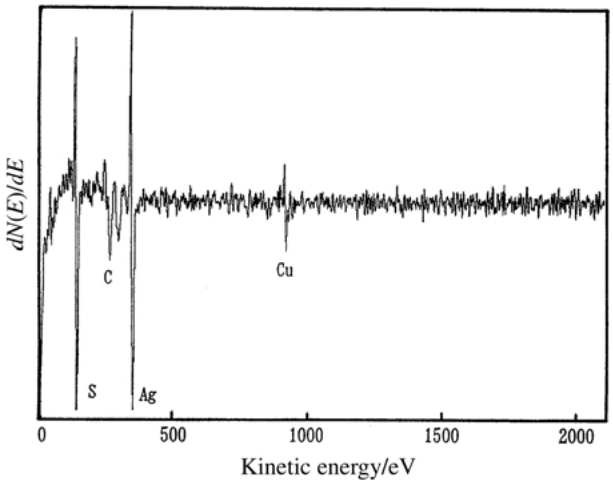

Figure 6 Auger survey spectrum of a small corrosion product formed on the Cu and Pd–rich coarse particle (microconstituent (a) in Fig. 1) after potentiostatic polarization at − 425 mV.

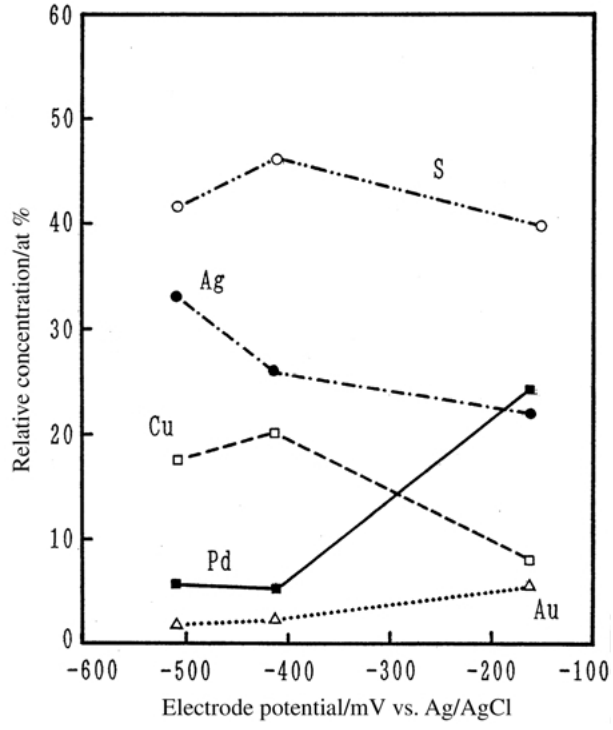

Figure 7 Relative concentrations of elements on the Ag–18Cu–15Pd–12Au alloy surface as a function of electrode potential, obtained by XPS measurement after potentiostatic polarization at each potential.

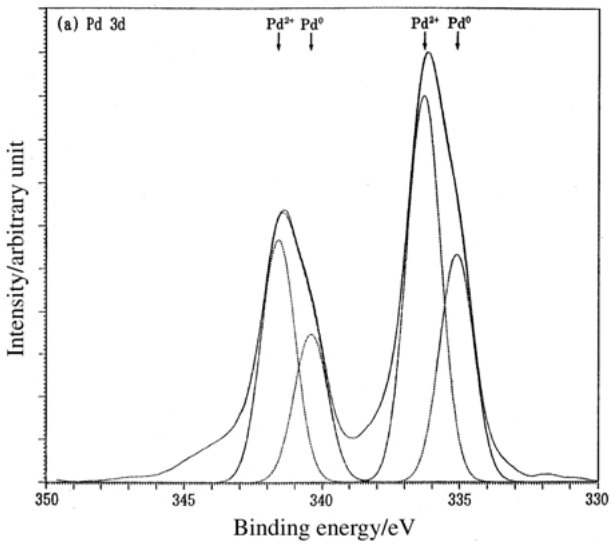

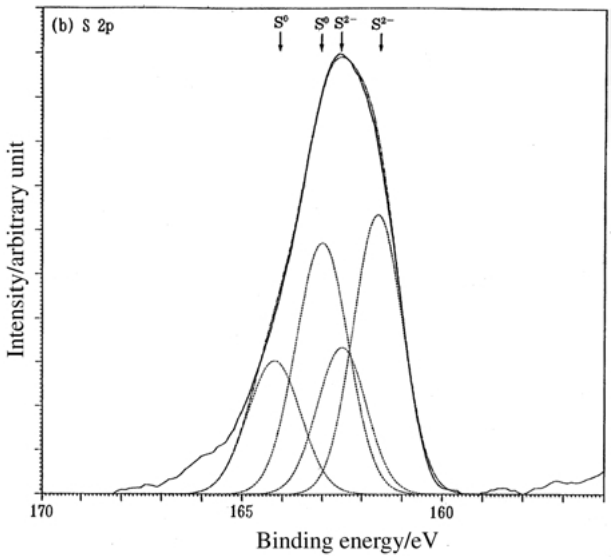

Figure 8 Pd 3d (a) and S 2p (b) spectra obtained from the Ag–18Cu–15Pd–12Au alloy surface after potentiostatic polarization at − 175 mV. Solid line: measured spectrum, dotted line: separated component spectra, chained line: sum of component spectra.

[11] and Ag–24.5Pd–13.5Cu–5.3Au alloy [12], and they formed during the solidification process followed by the subsequent solid–solid transformation [11]:

$$\text{Liquid} \rightarrow \alpha \text{ solid solution} \rightarrow \alpha_1 + \alpha_2 \rightarrow \alpha_1 + \alpha_2 + \text{PdCu}$$

The results of microprobe analyses suggest that the large particles with irregular shapes are Cu-rich α_1 phase and that Pd is enriched in this phase. The fine precipitate lamellae are also the α_1 phase because some of these precipitates are interconnected with large particles of the α_1 phase. The Widmanstätten precipitates both in the matrix and in the coarse particles are though to be the PdCu ordered phase because the amount of this phase is very small (Fig. 2) and this structure disappeared with solution treatment at 800 °C. The high content of Ag (55 mass%) and the high intensity of the α_2 diffraction peaks indicate that the matrix is the Ag-rich α_2 phase.

4.2. Anodic polarization behavior of the Ag–18Cu–15Pd–12Au alloy in an alkaline sulfide solution

The positions of the three current density peaks in the potentiodynamic polarization curve for the experimental alloy were identical to those for the commercial alloy, indicating that the mechanisms of corrosion in an alkaline sulfide solution were the same for the two alloys. The peak current densities for the experimental alloy, however, were markedly larger than those for the commercial alloy. This enhanced susceptibility of the experimental alloy to corrosion enabled us to elucidate the corrosion mechanism in a sulfide solution by characterizing the alloy surface, which was drastically changed in composition and morphology after potentiostatic polarization at different potentials. The anodic reactions that proceeding at peaks I–III are discussed below.

4.2.1. Anodic corrosion reactions involved at peak I

The Ag-rich matrix was preferentially corroded with the formation of Ag_2S at peak I. The Ag-rich α_2 phase was found to be the most susceptible to corrosion among the three phases in 0.1% Na_2S solution. This finding is in accordance with previous findings obtained by Niemi and Holland, who used light optical microscopy to examine the surface of an Ag–24.5Pd–13.5Cu–5.3Au alloy after immersion in 2% Na_2S solution for 45 h and found that tarnish attack took place only on the Ag-rich component [3].

The dominant sulfide species in 0.1% Na_2S solution ($pH = 12$) is HS^- [13] and the formation of Ag_2S occurs by the following reaction:

$$2Ag + HS^- + OH^- \rightarrow Ag_2S + H_2O + 2e \quad E = -0.771 \text{ V vs. Ag/AgCl} \tag{1}$$

The equilibrium potential (E) of reaction (1) in 0.1% Na_2S solution ($[OH^-] = 1.0 \times 10^{-2}$M, $[SH^-] = 1.3 \times 10^{-2}$M) was calculated using the Nernst equation [14]. The large granular deposits of Ag_2S, however, were not distributed uniformly over the whole matrix. They were found to be localized in specific areas of the Ag-rich matrix (Fig. 4 (a)). Fig. 9 shows high magnification images of the same area after the polarization at peak I for 15 min (a) and after etching in aqueous solution containing 5% KCN and 5% $(NH_4)_2S_2O_8$ (b). The images show large crystallized Ag_2S formed on the Ag-rich matrix with coarse, irregular-shaped α_1 lamellae, while small corrosion products formed on the Ag-rich matrix with fine α_1 lamellae and PdCu precipitates. It is evident from these findings that the Ag-rich matrix with coarse α_1 lamellae, which is located around the Cu and Pd-rich α_1 coarse particles, is the most corrosion-susceptible region.

X-ray diffractometry indicated that there were no crystalline Cu sulfides on the alloy surface after the potentiostatic polarization at peak I, although the sulfidation reaction of Cu is expected to occur at lower potential than that of Ag:

$$2Cu + HS^- + OH^- \rightarrow Cu_2S + H_2O + 2e \quad E = -1.007 \text{ V vs. Ag/AgCl} \tag{2}$$

This observation can be explained by the fact that Cu_2S is thermodynamically unstable and can be transformed to metallic Cu at peak I in 0.1% Na_2S solution ($[H^+] = 1.0 \times 10^{-12}$M):

$$Cu_2S + 4H_2O \rightarrow 2Cu + SO_4^{2-} + 8H^+ + 6e \tag{3}$$

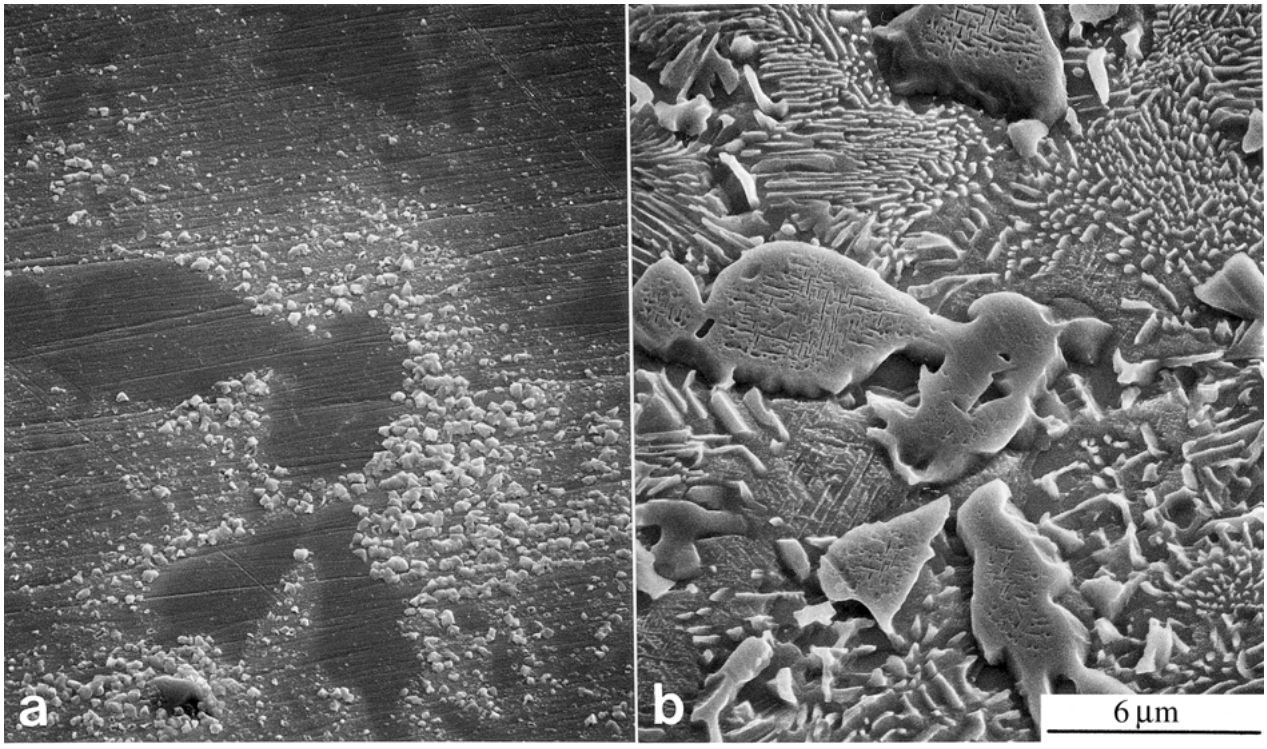

Figure 9 Secondary electron images of the Ag–18Cu–15Pd–12Au alloy surface after potentiostatic polarization at −520 mV for 15 min (a) and after etching in an aqueous solution containing 5% KCN and 5% $(NH_4)_2S_2O_8$ (b).

$$E = -0.642 + 0.0098 \log[SO_4^{2-}] \quad \text{V vs. Ag/AgCl}$$

Another reason for the absence of crystalline Cu sulfides is the higher Pd content in the Cu-rich phase than in the Ag-rich matrix (Fig. 1). The enrichment of Pd made the Cu-rich phase more corrosion-resistant than the Ag-rich phase and inhibited the formation of large crystalline deposits of Cu_2S.

4.2.2. Anodic corrosion reactions involved at peak II

The amount of deposited Ag_2S after potentiostatic polarization at peak II was markedly smaller than that at peak I (Fig. 4). The surface concentration of Ag at peak II was also lower than that at peak I (Fig. 7). These findings suggest that the Ag-rich matrix corrodes with the dissolution of Ag into the solution, which occurs in parallel with Ag_2S formation at peak II:

$$2Ag + HS^- + 6H_2O \rightarrow 2AgO^- + 13H^+ + SO_4^{2-} + 10e \quad (4)$$

$$E = -0.465 + 0.0059 \log[SO_4^{2-}][AgO^-]^{-2} \quad \text{V vs. Ag/AgCl}$$

In contrast to that of Ag, the surface concentration of Cu on the alloy surface after potentiostatic polarization at peak II was slightly higher than that at peak I (Fig. 7). The thermodynamically favorable reaction of Cu at peak II is the formation of Cu_2O:

$$2Cu + H_2O \rightarrow Cu_2O + 2H^+ + 2e \quad (5)$$
$$E = -0.435 \quad \text{V vs. Ag/AgCl}$$

Since the small deposits observed on the Cu and Pd-rich α_1 coarse particles were found to be Ag–Cu mixed sulfides, a thin film of Cu_2O probably formed on the Cu-rich phases, resulting in a slight increase in the surface concentration of Cu.

4.2.3. Anodic corrosion reactions involved at peak III

Pd was markedly enriched on the surface after potentiostatic polarization at peak III (Fig. 7). During the potentiostatic polarization, this surface enrichment of Pd could be achieved with the dissolution of Ag via reaction (4) and the dissolution of Cu by the following reaction:

$$Cu + 2H_2O \rightarrow HCu_2O^- + 3H^+ + 2e \quad (6)$$

$$E = -0.135 + 0.0295 \log[HCu_2O^-] \quad \text{V vs. Ag/AgCl}$$

The Pd 3d spectrum shown in Fig. 8(a) indicates the presence of Pd compound at the alloy surface. The thermodynamically favorable reactions of Pd at peak III are as follows:

$$Pd + HS^- + OH^- \rightarrow PdS + H_2O + 2e \quad (7)$$

$$E = -0.907 \quad \text{V vs. Ag/AgCl}$$

$$PdS + 5H_2O \rightarrow PdO + SO_4^{2-} + 10H^+ + 8e \quad (8)$$

$$E = -0.504 + 0.007 \log[SO_4^{2-}] \quad \text{V vs. Ag/AgCl}$$

Fig. 10 shows a Pd 3d spectrum obtained from the alloy surface after polarization at -175 mV for 15 min (a) together with Pd 3d spectra for high purity reagent of PdO (99.9%) (b) and metallic Pd (c). The spectrum peak at 336.3 eV obtained from the alloy surface after polarization at -175 mV does not correspond to PdO. Although chemical shift data for PdS has not been reported due to difficulty for preparing a high-purity sample of PdS suitable for XPS, the Pd 3d peak at 336.3 eV may be assigned to PdS. The fact that the concentration of S on the surface was higher than the concentrations of metal elements (Fig. 7) and the fact that more than 50% of S corresponds to metal sulfides (Fig. 8 (b)) also indicate the presence of PdS rather than PdO on the alloy surface. We therefore conclude that reaction (7) dominantly occurs with the formation of a Pd-rich sulfide film. The thickness of the Pd-rich surface sulfide film is estimated on the basis of the escape depth of Pd 3d photoelectrons to be less than 1 nm [15].

A current density peak was also observed for the inert Au electrode at -200 mV (near peak III), suggesting that the anodic current in this potential region is mostly attributed to the oxidation reactions of HS^-. The reactions proposed in the literature for iron and steel in alkaline sulfide solutions are oxidation of HS^- to elemental sulfur [16], soluble polysulfide [17], or $S_2O_3^{2-}$ [18]. The S 2p spectrum, which exhibits the presence of the adsorbed elemental sulfur on the alloy surface, also suggests that the oxidation of HS^- yielding sulfur occurs, at least in part at potentials above -175 mV.

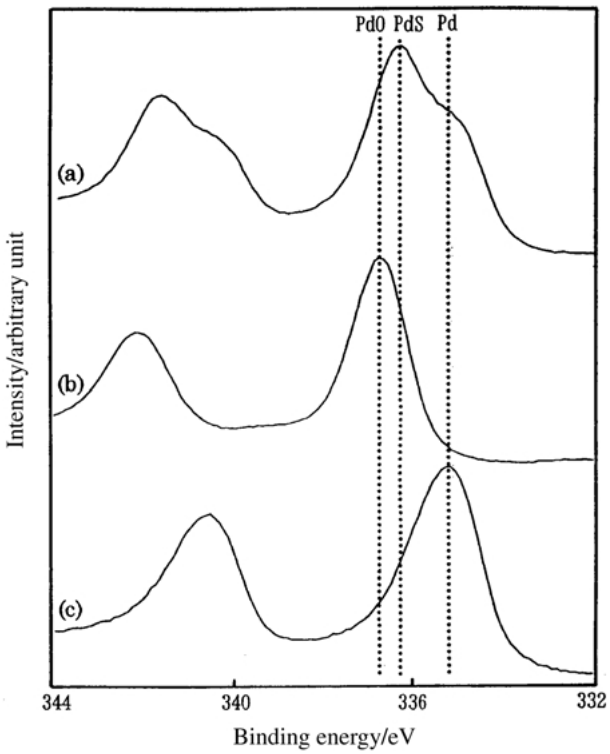

Figure 10 Pd 3d spectra obtained from the alloy surface after the polarization at -175 mV for 15 min (a), PdO (b), and the polished alloy with Ar^+ etching for 3 min (c).

4.3. Role of Pd in improvement of corrosion resistance at peak III

The amount of corrosion products at peak III was much smaller than the amounts formed at peaks I and II (Fig. 4), indicating that the corrosion resistance of the experimental alloy increased with enrichment of Pd on the surface. The authors [19] and Vaidyanathan *et al*. [4] have reported an improvement in the corrosion and tarnish resistance of Ag-based alloys in sulfide solution with an increase in Pd content. A small amount of Pd contained in an Au–Ag–Cu alloy has also been found to be effective in reducing the rate of tarnishing [20]. It is clear from these findings that Pd plays an important role in improvement of the corrosion and tarnish resistance of a dental noble alloy in sulfide environments. The mechanism by which Pd increases the resistance to corrosion and tarnishing, however, is not clear. Suoninen *et al*. [20] assumed that the enriched Pd on the surface of Au–Ag–Cu alloys decreased the diffusion of Ag and Cu from the bulk alloy to its surface and inhibited the formation of an $(Ag, Cu)_2S$ layer. However, further explanation of the stability of the enriched Pd layer itself is still needed because Pd is not thermodynamically inert in sulfide solutions but prone to corrode like Ag with the formation of its sulfide (reaction (7)).

In the present study, we demonstrated by XPS that a Pd-rich sulfide film of less than 1 nm in thickness formed on an alloy surface at peak III. This thin Pd-rich sulfide film, unlike the crystalline corrosion products of Ag_2S and Ag–Cu mixed sulfides, may be protective and responsible for the passivity of the alloy. A high level of corrosion resistance is thus attained by enrichment of Pd with the formation of a thin Pd-rich sulfide film, which enhances the passivity of the alloy in an alkaline sulfide solution. This finding implies that passivity of noble metal alloys, as well as nobility, is important for having a high level of corrosion resistance in a sulfide environment.

5. Conclusions

The anodic polarization behavior of an experimental Ag–18Cu–15Pd–12Au alloy in 0.1% Na_2S solution in relation to its microstructure at potentials from -650 to $+100$ mV was investigated. The Ag-rich matrix was found to be the most corrosion-susceptible phase and to preferentially corrode at potentials below -350 mV. Large crystallized Ag_2S particles formed on the Ag-rich matrix with coarse α_1 lamellae, while a small amount of fine deposits formed on the matrix with fine α_1 lamellae and PdCu precipitates. No large crystalline corrosion products of Cu_2S formed on the Cu and Pd-rich α_1 phase and the PdCu ordered phase at any of the potentials investigated. This finding is consistent with the fact that the thermodynamically stable species of Cu at -520, -425 and -175 mV are metallic Cu, Cu_2O and HCu_2O^-, respectively. At noble potentials above -175 mV, Pd was enriched on the alloy surface with the dissolution of Ag and Cu. Unlike the crystalline corrosion product of Ag_2S, the thin Pd-rich sulfide film on the alloy surface was protective and enhanced the passivity of the alloy. It has been found that passivity is an important phenomenon not only for base metal alloys but also for noble metal alloys to have high levels of corrosion and tarnish resistance in a sulfide environment. The findings regarding the anodic corrosion behavior of the experimental alloy obtained in this study would be useful for evaluating the corrosion resistance of an Ag–Pd–Cu–Au alloy in a sulfide environment and for developing noble metal alloys that possess high levels of resistance to corrosion and tarnishing.

Acknowledgment

This work was supported by a Grant in Aid for Scientific Research from the Ministry of Education, Science and Culture of Japan (No. 11671943).

References

1. K. MATSUDA, K. ENDO, K. YAMADA and H. OHNO, *J. Esthetic Dent*. **11** (1998) 58.
2. K. ENDO, Y. ARAKI and H. OHNO, *Dent. Mater. J.* **8** (1989) 46.
3. L. NIEMI and R. I. HOLLAND, *J. Dent. Res.* **63** (1984) 1014.
4. T. K. VAIDYANATHAN and A. PRASAD, *J. Dent. Res.* **60** (1981) 707.
5. R. M. GERMAN, D. C. WRIGHT and R. F. GALLANT, *J. Prosthet. Dent.* **47** (1982) 399.
6. L. A. O'BRIEN and R. M. GERMAN, *J. Mater. Sci.* **23** (1988) 3563.
7. B. R. LANG, S. H. BERNIER, Z. GIDAY and K. ASGAR, *J. Prosthet. Dent.* **48** (1982) 245.
8. K. ENDO, Y. ARAKI, I. KAWASHIMA, Y. YAMANE, H. OHNO and K. MATSUDA, *Higashi Nippon Dent. J.* **8** (1989) 49.
9. K. IIJIMA, I. MATSUDA and H. HONMA, *Tohoku Univ. Dent. J.* **10** (1991) 101.
10. R. I. HOLLAND, *Scand. J. Dent. Res.* **19** (1991) 95.
11. H. OHNO and E. SHIOKAWA, in ''Microstructure of Dental Alloys'' (Nagasue Publ., Tokyo, 1978) p. 226.
12. L. NIEMI and H. HERO, *J. Dent. Res.* **63** (1984) 149.
13. M. POURBAIX, in ''Atlas of Electrochemical Equilibria in Aqueous Solutions'' (National Association of Corrosion Engineers, Houston, 1974) p. 546.
14. K. R. TRETHEWEY and J. CHAMBERLAIN, in ''Corrosion for Students of Science and Engineering'' (Longman Scientific and Technical, Essex, 1988) p. 66.
15. D. BRIGGS and M. P. SEAH, in ''Practical Surface Analysis by Auger and X-ray Photoelectron Spectroscopy'' (John Wiley and Sons, New York, 1985) p. 186.
16. H. KAESCHE, *Werkstoffe Korros.* **21** (1970) 185.
17. D. W. SHOESMITH, M. G. BAILEY and B. IKEDA, *Electrochimica Acta* **23** (1978) 1329.
18. D. TROMANS *J. Electrochem. Soc*. **127** (1980) 1253.
19. K. ENDO, M. SUZUKI, H. OHNO and K. MATSUDA, *Bull. Kanagawa Dent. Col*. **26** (1998) 114.
20. E. SUONINEN, H. HERO and E. MINNI, *J. Biomed. Mater. Res.* **19** (1985) 917.

Received 1 March
and accepted 21 October 2002